Semmling, A. M., Beyerle, G., Stosius, R., Dick, G., Wickert, J., Fabra, F., Cardellach, E., Ribó, S., Rius, A., Helm, A., Yudanov, S. B., d'Addio, S. (2011): Detection of Arctic Ocean tides using interferometric GNSS-R signals. - Geophysical Research Letters, 38, L04103

DOI: 10.1029/2010GL046005

Detection of Arctic Ocean tides using interferometric GNSS-R signals

A. M. Semmling,[1] G. Beyerle,[1] R. Stosius,[1] G. Dick,[1] J. Wickert,[1] F. Fabra,[2] E. Cardellach,[2] S. Ribó,[2] A. Rius,[2] A. Helm,[3] S. B. Yudanov,[4] and S. d'Addio[5]

Received 2 November 2010; revised 9 January 2011; accepted 11 January 2011; published 17 February 2011.

[1] This paper evaluates the usage of reflected GPS signals for Earth observations to study changes of sea level and sea-ice in remote sensing. In a coastal setup, ~670 m above Disko Bay (Greenland), signals with different carriers L1 and L2 were recorded. A method is presented that analyses the interferometric phase between the reflected and the direct signals and derives the height of the reflecting surface. The analysis includes a ray tracing and an estimation of signal coherence. It is shown that coherent reflections are related to sea-ice coverage. Absolute heights are derived with a time interval of ~30 min. The altimetric results show semidiurnal tides that are validated using the AODTM-5 tide model. The residual height has a mean of 9.7 cm for L1 and 22.9 cm for L2. The dispersion is not significant but a significant tropospheric bias is detected with an error of up to 20 cm. **Citation:** Semmling, A. M., et al. (2011), Detection of Arctic Ocean tides using interferometric GNSS-R signals, *Geophys. Res. Lett.*, *38*, L04103, doi:10.1029/2010GL046005.

1. Introduction

[2] Reflections of GPS signals have been widely used for remote sensing of the Earth surface. The large number of signals and the high coverage reveal new perspectives for Earth observations, the detection of eddies [*Ruffini et al.*, 2004] or tsunamis [*Stosius et al.*, 2010] has been investigated. Next to ocean altimetry, GNSS reflectometry (GNSS-R) has a large potential for ice and snow remote sensing. Here we concentrate on the L-band carrier of the GPS signal for interferometric analysis. For a standard geodetic receiver snow depths could be derived on a local scale [*Larson et al.*, 2009]. Dedicated occultation receivers in space provide reflections on a global scale [*Beyerle and Hocke*, 2001]. An interferometric method was used to reach a submeter sensitivity on surface heights using GPS occultation data from the CHAMP satellite [*Cardellach et al.*, 2004]. But occultation data is restricted to grazing angles. Therefore the number of observations and the altimetric precision are limited [*Rius et al.*, 2010]. Dedicated GNSS-R receivers have been designed to overcome these limitations [*Lowe et al.*, 2002; *Nogues-Correig et al.*, 2007]. We use a prototype of a geodetic JAVAD receiver that was modified for GNSS-R, the GORS receiver [*Helm et al.*, 2007]. This paper presents interferometric results retrieved from the GORS receiver. The paper is sectioned as follows: the experimental setup, the acquisition of the interferometric phase, the calculation of an altimetric model and the height retrieval are described in section 2. Results regarding the coherence of observations, the altimetric results and their validation are given in section 3. Error sources and future implications are discussed in section 4.

2. Experiment and Data Analysis

2.1. Setup

[3] In a GPS Sea-Ice campaign initiated by ESA a ground based experiment was set up on a cliff ~670 m above Disko Bay near Godhavn/Greenland (69.27°N, 53.54°W). The location offers an exposed position to study sea-ice formation and sea level changes in the arctics. Two independent GNSS-R equipments were deployed: the GORS receiver and a dedicated receiver called GOLD-RTR [*Nogues-Correig et al.*, 2007]. *Fabra et al.* [2010] gives an overview about GOLD-RTR results. Here, the GORS experiment is described. The characteristic specular geometry of the reflection is shown in Figure 1a. Observations of a single reflection track recur with a nearly siderial period ~24 h [*Agnew and Larson*, 2007]. During continuous observation of reflections (Nov. 2008–Jan. 2009) about 50 different tracks were recorded successively every day, see Figure 1b. Accordingly, the period between the observations decrease to ~25 min. To reach this optimum time resolution, a spreading of the footprints is accepted. The aliasing in tide observations using a single reflection track can be resolved, cf. (F. Fabra et al., Phase altimetry with dual polarization GNSS-R over sea ice, submitted to *IEEE Transactions of Geoscience and Remote Sensing*, 2010).

2.2. Interferometric Phase

[4] The setup in Figure 1a uses only one tilted antenna to acquire the direct and the reflected signal in a right-handed circular polarization (RHCP). The receiver is equipped with a master channel for the direct signal and a slave channel for the reflected signal. They track the same satellite at different code delays. The master tracks the code delay of the direct correlation peak τ_0. The reflected peak has an additional delay $\Delta\tau$. Using an a priori model τ_A, the

[1] Department of Geodesy and Remote Sensing, Deutsches GeoForschungsZentrum Potsdam, Potsdam, Germany.
[2] ICE, IEEC, CSIC, Barcelona, Spain.
[3] EADS Deutschland GmbH, Immenstaad, Germany.
[4] Javad GNSS, Moscow, Russia.
[5] European Space Research and Technology Centre, Noordwijk, Netherlands.

0094-8276/11/2010GL046005

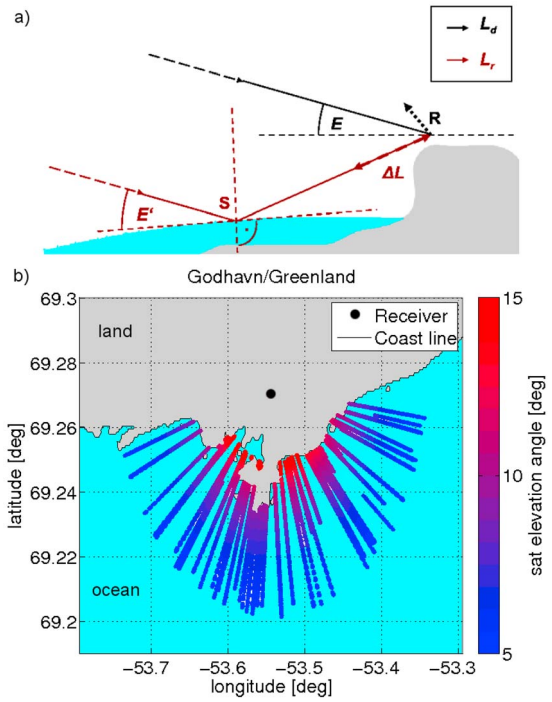

Figure 1. (a) Specular geometry of the reflection. The path difference ΔL carries altimetric information. The satellite elevation is different at the receiver position (R) and the specular point (S). In the following we refer to E as the satellite elevation angle. The dotted arrow shows the tilted antenna axis. (b) The tracks of all reflections per day. Their range is limited by $E > 5°$.

slave tracks the reflection delay $\Delta\tau$. Complex models γ_{mst} and γ_{slv} are derived according to *Treuhaft et al.* [2001].

$$\gamma_{mst}(\tau_0) = e^{i\phi_0}\left[A_d + A_r e^{ik_0\Delta L}\Lambda(\Delta\tau)\right]$$

$$\gamma_{slv}(\tau_0 + \tau_A) = e^{i\phi_0}\left[A_d\Lambda(\tau_A) + A_r e^{ik_0\Delta L}\Lambda(\tau_A - \Delta\tau)\right]$$

$$\gamma_{int} = \frac{\gamma_{slv} - \Lambda(\Delta\tau)\gamma_{mst}}{1 - \Lambda^2(\Delta\tau)} \quad (1)$$

$$\propto A_r e^{ik_0\Delta L} \quad (2)$$

The assumption $\Delta\tau \approx \tau_A$ leads to the interferometric model γ_{int}, that contains the essential information given by the path difference $\Delta L = L_r - L_d$. The indices $_d$ and $_r$ denote the direct and reflected signal respectively. The amplitude and the optical phase path are denoted A and L. The carrier wave number is k_0 and $\Lambda(\tau)$ denotes the triangular autocorrelation function of the GPS code. In contrast to *Treuhaft et al.* [2001], the phase offset ϕ_0 is constant. Phase changes of the direct signal were removed by the tracking algorithm. If the direct and the reflected signals are coherent, interference is observed in the signal γ_{int}, see Figure 2a. Then the interferometric phase is continuous and a *maximum phase gradient* algorithm [*Ghiglia and Pritt*, 1998] is used to determine the number of coherent observations.

2.3. Altimetric Model

[5] The paths L_d and L_r are calculated using a ray tracing. An altimetric model γ_{alt} is derived, that implicitly depends on the ellipsoidal surface height H.

$$\gamma_{alt} = \exp\left[-i\tfrac{2\pi}{\lambda}\left(L_r(\vec{R},\vec{X},H,n) - L_d(\vec{R},\vec{X},n)\right)\right] \quad (3)$$

λ denotes the wavelength of the L-band carrier. The position of the receiver $\vec{R}$ is derived by precise analysis of the direct signal [*Gendt et al.*, 1998]. For the position of the transmitter $\vec{X}$ broadcast ephemerides are used. Meteorological data provided by the European Centre for Medium-Range Weather Forecasts (ECMWF) is used to determine the non-dispersive refractivity n in the neutral atmosphere according to *Bevis et al.* [1994]. Dispersive refraction in the ionosphere is neglected. Starting at a reference height provided by the Earth Gravitational Model (EGM96), γ_{alt} is computed for different heights H_i separated by 1 m steps.

2.4. Height Retrieval

[6] The basic idea of this method is to find a model $\gamma_{alt}(H)$ that tracks the variations in γ_{int}, see Figure 2a. A tracked signal is obtained by a complex product $\gamma_i = \gamma_{int} \cdot [\gamma_{alt}(H_i)]^*$. Provided that all other parameters are sufficiently modelled, the true surface height H_S is determined when the mean frequency of the tracked signal vanishes. The mean over the time

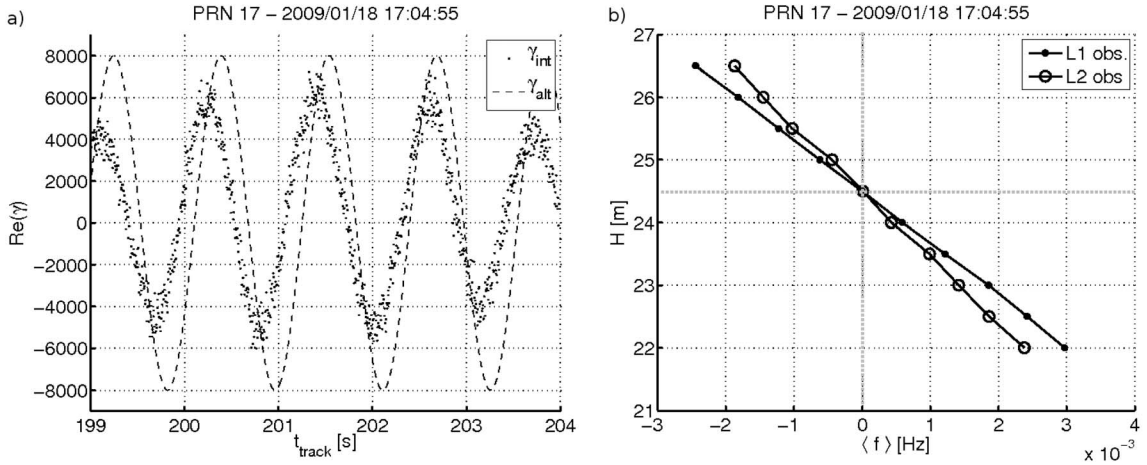

Figure 2. (a) The real part of a coherent interferometric signal γ_{int} and the altimetric model γ_{alt}. The interference pattern shows almost the same frequency. (b) The modelled ellipsoidal height H vs. the mean frequency of the tracked phase $\langle f \rangle$. The derived surface height H_S is equal for L1 and L2 observations, there is no dispersion.

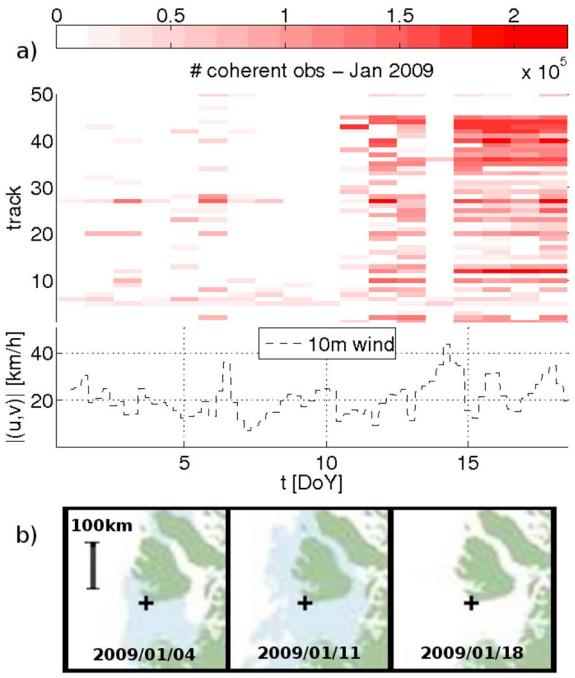

Figure 3. (a) The number of coherent observations and the wind speed 10 m above the surface for the first half of January 2009. The tracks are sorted by azimuth. The track number is assigned clockwise from East (cf. Figure 1). (b) Maps showing the sea-ice coverage in Disko Bay. Disko Island and the coast are green, areas in blue refers to open water and those in white to sea-ice. The observed area of the setup is marked with a cross. Maps provided by DMI weekly ice charts.

of the track is denoted $\langle\cdot\rangle$. To compute the mean frequency $\langle f_i\rangle = \langle d\varphi_i/dt\rangle$, the unwrapped phase $\varphi_i = \mathfrak{U}\{\arg(\gamma_i)\} + N$ is derived. $\arg(\gamma_i)$ denotes the phase angle of γ_i. The unwrap operation $\mathfrak{U}\{\}$ corrects the phase angle by adding $\pm 2\pi$, when jumps greater than the tolerance of π occur. The constant ambiguity N is unimportant for the mean frequency of the track. A linear relation between the height levels H_i and $\langle f_i\rangle$ is observed, as shown for L1/L2 observations of PRN 17 in Figure 2b. A linear fit yields the surface height $H_{fit}(0) = H_S$.

$$H_{fit}(\langle f\rangle) = a_{fit}\langle f\rangle + H_s \tag{4}$$

The slope is denoted a_{fit}. The standard deviation $\sigma(f) = \langle (f(t) - \langle f\rangle)^2\rangle$ is used to remove outliers. Only heights H_S are considered with $\sigma(f) < 1$ mHz.

3. Results

[7] The altimetric performance depends on the occurrence of coherent observations. An overview of coherence for the daily recurring tracks is shown in Figure 3a. Three maps from the Danish Meteorological Institute (DMI) in Figure 3b give an overview on sea-ice coverage in Disko Bay. Coincidence of coherence and sea-ice is detected mid of January 2009. Similar conclusions are given by Fabra et al. (submitted manuscript, 2010), [Belmonte Rivas et al., 2010]. According to precise ice charts, sea-ice concentration close to Godhavn reaches >90% between 2009/01/11 and 2009/01/18. For 2009/01/14 a short loss of coherence coincides with a peak in the local surface wind speed of more than 40 km/h (ECMWF database), see Figure 3a. It indicates a higher surface roughness of the ocean that influences coherence in GNSS-R, as described by *Soulat et al.* [2004]. For the period 2009/01/15 to 2009/01/18 almost all tracks show coherence that yields altimetric results. The corresponding time series is dense enough to resolve semidiurnal tides, see Figure 4. The modelled ocean height H_M results from the sum of a permanent geoid undulation w.r.t. WGS84 (given by EGM96) and tide variations predicted by the Arctic Ocean Tidal Forward Model (AODTM-5) [*Padman et al.*, 2002]. The derived surface heights H_S are restricted to $\sigma(f) < 1$ mHz, which is an arbitrary threshold for the application of the model. The residual height $\Delta H = H_S - H_M$ has a mean of 9.7 cm for L1 and 22.9 cm for L2. The RMS of the residual height is 35.0 cm for L1 and 47.3 cm for L2. The RMS error of the AODTM-5 model for Disko Bay is about 12.5 cm. A significant dispersion in L1 and L2 observations, e.g., due to ionospheric refraction, is not observed.

4. Discussion

[8] A limiting factor of this method is signal coherence. If coherence is lost, $\sigma(f)$ exceeds the threshold. For this setup sufficient coherence is only observed at low wind speed and in the presence of sea-ice mid of Jan. 2009. A higher percentage of coherent observations could be obtained using a higher gain in a different antenna layout. For the heights derived here, the RMS deviation indicates unmodelled errors. In general, significant error sources are located below the receiver height. Far above the receiver, direct and reflected signals are affected almost identically and errors cancel out. Simulations predict an ionospheric bias of only 1 cm. The error related to GPS broadcast ephemerides is even lower. Due to dry arctic conditions in Jan. 2009 fluctuations in the wet tropospheric path delay were rather low. The relative error in tropospheric delay was <1%. Simulations predict a corresponding error up to 20 cm in the altimetric results at lowest elevations of 5°. The multipath error, due to reflections close to the antenna setup, is mitigated by a minimum length of observations, for more details see Fabra et al. (submitted

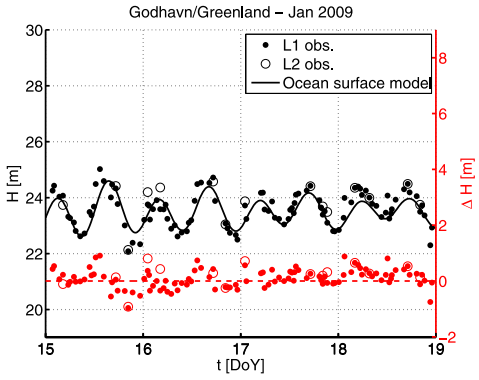

Figure 4. The ellipsoidal height H w.r.t. WGS84 for the day of the year in Jan. 2009. The derived surface height for L1/L2 observations and the ocean surface height model are plotted in black. The residual height ΔH for L1/L2 observations is plotted in red.

manuscript, 2010). An error is expected due to the simplified surface model. Undulations of the surface along the track and between different tracks, see Figure 1b remain unresolved. The appearance of icebergs, e.g., (calved from Jacobhavn glacier) will affect the reflection path but remain unresolved. Provided that ancillary data on the geoid and the sea-ice state is available and the elevation > 10°, the sea-ice freeboard height could be considered. The results show, that H_S lies above the model H_M in the later period, cf. Figure 4. It indicates a residual bias similar to the sea-ice freeboard but it is not significant due to the large RMS of ΔH. The high coverage and time resolution in general has important implications in sea-ice and sea level monitoring. A passive shore-mounted instrument offers continuous observations at low operating costs and covers coastal zones that are inaccessible for spaceborne radar altimeters. In contrast to tide gauges no in-situ access is needed. However, to establish the method for airborne and spaceborne missions further research is required.

[9] **Acknowledgments.** We are grateful for the meteorological data from ECMWF. For ice charts and further support we thank Martin Sørensen and the colleagues from DMI. For TEC estimation we thank Norbert Jakowski and the colleagues from DLR Neustrelitz. R. König and other colleagues at GFZ are gratefully acknowledged for the provision of GPS ephemerides. This study was funded by ESA within the *GPS Sea Ice and Dry Snow* project (ESA CN 21793/08/NL/ST) and by GFZ. E.C. is under the Spanish *Ramón y Cajal* Program. E. Calais thanks two anonymous reviewers.

References

Agnew, D. C., and K. M. Larson (2007), Finding the repeat times of the GPS constellation, *GPS Solut.*, *11*, 71–76.

Belmonte Rivas, M., J. A. Maslanik, and P. Axelrad (2010), Bistatic scattering of GPS signals off Arctic sea ice, *IEEE Trans. Geosci. Remote Sens.*, *48*(3), 1548–1553.

Bevis, M., S. Businger, S. Chiswell, T. A. Herring, R. A. Anthes, C. Rocken, and R. H. Ware (1994), GPS meteorology: Mapping zenith delays onto precipitable water, *J. Appl. Meteorol.*, *33*, 379–386.

Beyerle, G., and K. Hocke (2001), Observation and simulation of direct and reflected GPS signals in Radio Occultation Experiments, *Geophys. Res. Lett.*, *28*, 1895–1898.

Cardellach, E., C. O. Ao, M. de la Torre Juárez, and G. A. Hajj (2004), Carrier phase delay altimetry with GPS-reflection/occultation interferometry from low Earth orbiters, *Geophys. Res. Lett.*, *31*, L10402, doi:10.1029/2004GL019775.

Fabra, F., et al. (2010), Monitoring sea-ice and dry snow with GNSS reflections, in *Proceedings of 2010 IEEE International Geoscience and Remote Sensing Symposium*, pp. 3837–3840, Inst. Electr. and Electron. Eng., New York.

Gendt, G., G. Dick, and W. Soehne (1998), GFZ analysis center of the IGS—Annual report 1998, technical report, Jet Propul. Lab., Pasadena, Calif.

Ghiglia, D. C., and M. D. Pritt (1998), *Two-Dimensional Phase Unwrapping: Theory, Algorithms, and Software*, Wiley, New York.

Helm, A., O. Montenbruck, J. Ashjaee, S. Yudanov, G. Beyerle, R. Stosius, and M. Rothacher (2007), GORS—A GNSS occultation, reflectometry and scatterometry space receiver, in *ION GNSS 2007*, pp. 2011–2021, Inst. of Navig., Fort Worth, Tex.

Larson, K. M., E. D. Gutmann, V. U. Zavorotny, J. J. Braun, M. W. Williams, and F. G. Nievinski (2009), Can we measure snow depth with GPS receivers?, *Geophys. Res. Lett.*, *36*, L17502, doi:10.1029/2009GL039430.

Lowe, S. T., et al. (2002), A delay/doppler-mapping receiver system for GPS-reflection remote sensing, *IEEE Trans. Geosci. Remote Sens.*, *40*(5), 1150–1163, doi:10.1109/TGRS.2002.1010901.

Nogues-Correig, O., E. Cardellach, J. Sanz Campderros, and A. Rius (2007), A GPS-reflections receiver that computes doppler/delay maps in real-time, *IEEE Trans. Geosci. Remote Sens.*, *45*(1), 156–174, doi:10.1109/TGRS.2006.882257.

Padman, L., H. A. Fricker, R. Coleman, S. Howard, and L. Erofeeva (2002), A new tide model for the Antarctic ice shelves and seas, *Ann. Glaciol.*, *34*, 247–254.

Rius, A., E. Cardellach, and M. Martin-Neira (2010), Altimetric analysis of the sea surface GPS reflected signals, *IEEE Trans. Geosci. Remote Sens.*, *10*(4), 2119–2127, doi:10.1109/TGRS.2009.2036721.

Ruffini, G., F. Soulat, M. Caparrini, O. Germain, and M. Martín-Neira (2004), The Eddy Experiment: Accurate GNSS-R ocean altimetry from low altitude aircraft, *Geophys. Res. Lett.*, *31*, L12306, doi:10.1029/2004GL019994.

Soulat, F., M. Caparrini, O. Germain, P. Lopez-Dekker, M. Taani, and G. Ruffini (2004), Sea state monitoring using coastal GNSS-R, *Geophys. Res. Lett.*, *31*, L21303, doi:10.1029/2004GL020680.

Stosius, R., G. Beyerle, A. Helm, A. Hoechner, and J. Wickert (2010), Simulation of space-borne tsunami detection using GNSS-reflectometry applied to tsunamis in the Indian Ocean, *Nat. Hazards Earth Syst. Sci.*, *10*(6), 1359–1372.

Treuhaft, R. N., S. T. Lowe, C. Zuffada, and Y. Chao (2001), 2-cm GPS altimetry over Crater Lake, *Geophys. Res. Lett.*, *28*, 4343–4346.

G. Beyerle, G. Dick, M. Semmling, R. Stosius, and J. Wickert, Department of Geodesy and Remote Sensing, GeoForschungsZentrum Potsdam, Telegrafenberg, D-14473 Potsdam, Germany. (maxsem@gfz-potsdam.de)

E. Cardellach, F. Fabra, S. Ribó, and A. Rius, ICE, IEEC, CSIC, Campus UAB, Fac. Ciéncies, Torre C5-parell, 2on pis, E-08193 Barcelona, Spain.

S. d'Addio, European Space Research and Technology Centre, Keplerlaan 1, NL-2200 AG Noordwijk, Netherlands.

A. Helm, EADS Deutschland GmbH, Claude-Dornier-Strasse, D-88090 Immenstaad, Germany.

S. Yudanov, Javad GNSS, LLC, Chapayevskiy per. 3, Moscow 125252, Russia.